DYNAMIC SPACE CHARGE CALCULATIONS FOR HIGH INTENSITY BEAMS IN RINGS*

J. A. Holmes, J. D. Galambos, D. Jeon, D. K. Olsen, J. W. Cobb,
SNS Building, Oak Ridge National Laboratory, Oak Ridge, TN 37831-8218
M. Blaskiewicz, A. U. Luccio, and J. Beebe-Wang,
Brookhaven National Laboratory, Upton, NY 11973, USA

Abstract

Space-charge-induced emittance growth and halo generation could lead to unacceptably high beam loss in high intensity rings, such as the SNS [1]. In such accelerators, uncontrolled losses to the walls as small as one part in 10^4 would lead to activation, making maintenance difficult. For this reason it is essential to understand the effects of space charge on beam dynamics, and halo generation in particular, in high intensity rings. We have undertaken the study of space charge dynamics in high intensity rings using a particle tracking approach, with self-consistent evaluation of the space charge forces through a particle-in-cell model. Because of the stringent loss requirements, it is necessary to thoroughly guarantee the reliability of these calculations to high precision through comparison with experiments and through convergence studies. In this paper we present the results of convergence studies in the parameters of the model, namely, the number of macroparticles, the resolution in the adopted FFT algorithm, the smoothing parameter, and the time step size. Although present calculations have been extended to more than 10^5 macroparticles on individual UNIX workstations, it will be necessary to increase another one to two orders of magnitude to obtain the necessary precision. To accomplish this, we have constructed and are now using a LINUX parallel computer from low cost components.

1 INTRODUCTION

The operating requirements of some new rings, such as the Spallation Neutron Source (SNS) accumulator ring, include high intensity beams, low uncontrolled losses, and a considerable beam flight path in the ring. In these circumstances, space-charge-induced halo generation is a potential loss mechanism, and requires study. High intensity rings are characterized by the separation of longitudinal and transverse scales. In SNS, for example, the longitudinal bunch length is on the order of 100*m*, compared with transverse beam dimensions of a few *cm*; and the longitudinal tune is about 10^{-3}, compared with transverse tunes of about 5.8. For this reason it is possible, with good approximation, to separate the longitudinal and transverse dynamics in high intensity rings and, for the study of space charge effects, to consider the transverse dynamics. This simplification allows the description in terms of four, rather than six, dimensional phase space, which necessitates a smaller solution space to obtain a given numerical precision than is required in six dimensions.

In order to study transverse beam dynamics in high intensity rings, and space charge effects in particular, we have adopted a particle-tracking approach [2]. The integration scheme is chosen to be second order symplectic, with a matrix representation of all linear focusing elements, including dispersion, and the inclusion of all nonlinear effects as kicks. Our treatment of space charge uses a particle-in-cell (PIC) model [2] with fast Fourier transforms (FFTs) to evaluate the forces. This is carried out in a modified version of the particle tracking and injection code, ACCSIM [3], and in a new code, SAMBA, which we are now developing.

In PIC calculations, numerical convergence and accuracy must be carefully assured. We present in this paper the results of convergence studies in the parameters of the model. Section 2 presents the equations and numerical solution of the model; Section 3 presents the convergence results; and Section 4 contains discussion and conclusions.

2 EQUATIONS AND NUMERICAL SOLUTION

The essence of our transverse particle tracking model is the following pair of dynamic equations for the macroparticle coordinates x and y :

$$\begin{aligned} x'' + K_x(s)x &= F_x^{sc} + F_x^{nl} + \frac{1}{\rho(s)}\frac{\delta p}{p_0} \\ y'' + K_y(s)y &= F_y^{sc} + F_y^{nl} \end{aligned} \qquad (1)$$

where s is the azimuthal coordinate, $K_{x,y}(s)$ are the linear magnet focusing strengths, $F_{x,y}^{sc}(s)$ are the space charge forces, $F_{x,y}^{nl}(s)$ are the external nonlinear forces, and $\frac{1}{\rho(s)}\frac{\delta p}{p_0}$ is the dispersion term. The linear focusing forces, external nonlinear forces, and bending radius are all dependent on the lattice; while the momentum

deviation $\frac{\delta p}{p_0}$ is determined by the longitudinal dynamics. The space charge forces are evaluated self-consistently:

$$F_x^{sc} = P\sum_{i=1}^{N} \frac{x - x_i}{(x-x_i)^2 + (y-y_i)^2 + \varepsilon^2}$$
$$F_y^{sc} = P\sum_{i=1}^{N} \frac{y - y_i}{(x-x_i)^2 + (y-y_i)^2 + \varepsilon^2} \quad (2)$$

where the summation is over the number of macroparticles N, $P = \frac{2Z^2 r_p \lambda}{\gamma^3 \beta^2 AN}$, Z is the beam charge number, A is the mass number, r_p is the classical radius of the beam particle, γ and β are the relativistic kinematic parameters, λ is the longitudinal beam particle density, and ε is a numerical smoothing parameter.

The numerical model solves the dynamic equations using an explicit, second order, symplectic integration scheme:

- Divide the lattice into N_{az} linear elements (drifts, bends, quadrupoles);
- Transport macroparticles through these elements using a transport matrix approach, including dispersion;
- Treat nonlinear forces as kicks, applied at the ends of linear elements with strengths appropriate to a second order symplectic scheme;
- External nonlinear forces can be applied independently to each macroparticle;
- Space charge forces involve interaction of all beam macroparticles, and require special treatment.

The space charge forces are evaluated as nonlinear kicks using a PIC model and FFTs:

- At each azimuth s, select a regular rectangular (x, y) mesh of $N_{FFT} \times N_{FFT}$ points, centered on the beam. Because of the periodicity of the FFT, the mesh must be at least twice the extent of the beam in each direction;
- Obtain the particle density on the mesh by bilinear distribution of the macroparticle charges to adjacent mesh points;
- Obtain the FFT of space charge forces at mesh points as the convolution of the FFT of the particle density that of the force due to a unit charge. The inverse FFT of this quantity gives the space charge forces on the mesh points.
- Obtain the space charge force on each macroparticle as a bilinear interpolation of the forces at the mesh points to the location of the macroparticle.

The advantage of using this FFT procedure is one of speed, with the number of operations scaling as N for particle distribution and force interpolation and as $N_{FFT} \times \ln(N_{FFT})$ for the transforms. A limitation of the FFT is that it is not conducive to the inclusion of wall effects.

The study of space charge using this numerical model involves a number of parameters:

- N the number of macroparticles;
- N_{FFT} the spatial resolution (grid parameter for the FFT algorithm);
- ε the smoothing parameter; and
- N_{az} the azimuthal integration step size.

We now study the convergence properties of an example calculation with respect these parameters.

3 CONVERGENCE OF THE MODEL FOR AN EXAMPLE CASE

We now study the effect of the parameters of the numerical scheme on the convergence of the model for an example case, namely halo generation by the parametric resonance [4] in a doublet lattice. We consider a doublet lattice with fourfold symmetry similar to the SNS FODO lattice, length 220.668*m*, having linear focusing only (48 quadrupoles, 32 sector bends, and 80 drifts) and bare tunes of ν_x=5.85 and ν_y=5.70. We consider a coasting beam with a K-V distribution, energy and energy spread E_0=1*GeV*, $\Delta E_{\max}$=9.4*MeV*, ΔE_{rms}=4.7*MeV*, x and y emittances $\varepsilon_{x,y} = 100\pi$ *mm-mrad*, and number of particles $N = 3.08\times10^{14}$. The initial beam is rms mismatched, resulting in envelope oscillations of about 10% around the matched values. We follow the subsequent evolution for 1250 turns.

The evolution is observed to be as follows: Because the beam is mismatched envelope oscillations occur, as shown in Fig. 1 which plots the beam averages of $<(x-<x>)^2>$ and $<(y-<y>)^2>$ ($<(\Delta x)^2>$ and $<(\Delta y)^2>$). Because the y tune is less than the x tune, the focusing is slightly weaker in y than in x, and through coupling the oscillation energy is transferred from the x direction into the y direction. As the beam relaxes some particles cross the separatrix of the parametric resonance, driven by the oscillations in $<(\Delta y)^2>$, becoming halo particles and leading to a growth in the rms y emittance (Fig. 2). This halo

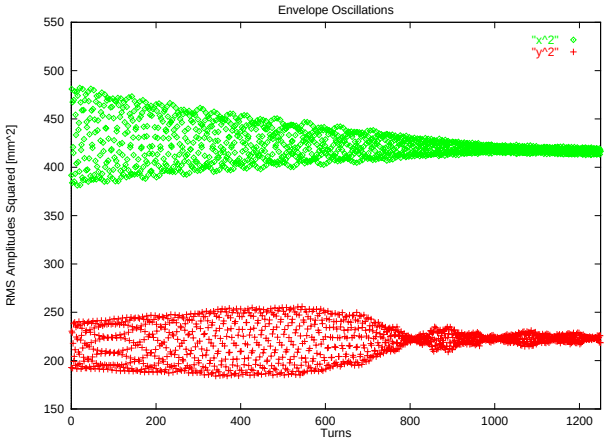

Figure 1. Average values of $<(\Delta x)^2>$ and $<(\Delta y)^2>$ plotted once each turn and showing envelope oscillations.

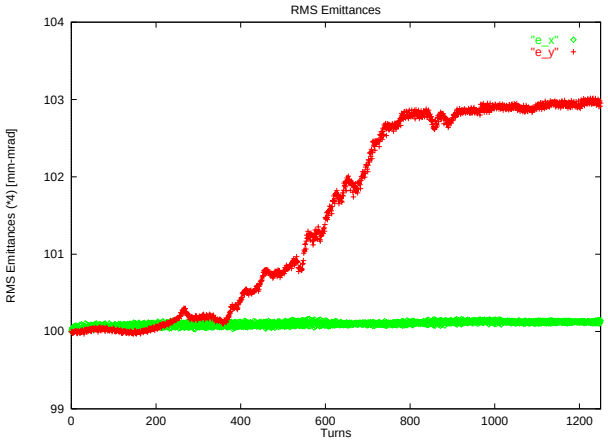

Figure 2. Transverse rms emittances ε_x and ε_y versus turn number.

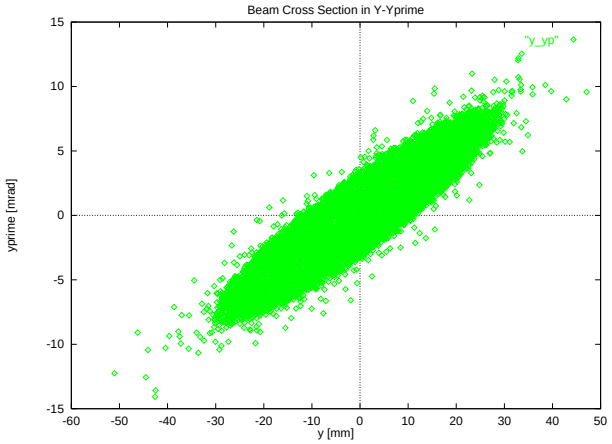

Figure 3. Final beam distribution in $y - y'$ phase space showing beam core and halo particles.

generating process removes energy from the envelope oscillations, which then diminish. As this driving force is removed, the instability saturates (Fig. 2) with the beam in a new steady state with halo. Figure 3 plots the final beam cross section in the $y - y'$ phase plane.

That the observed evolution is a result of physics, and not a numerical instability, was tested by carrying out the same calculation with the only difference being the method for distributing the charge to the FFT grid. In this latter method, each particle is regarded as a representative of a population of macroparticles, all having the same action values (J_x, J_y) but distributed uniformly over betatron oscillation phases (ϕ_x, ϕ_y). In this "phase averaged" model envelope oscillations are suppressed so that the parametric resonance is not driven, but no changes are made to numerical methods or parameters. The result of the phase averaged calculation is emittance conservation and no halo generation, as expected for a stable numerical scheme. This indicates that the observed instability is a result of the dynamics.

We also performed convergence studies in the four numerical parameters N, N_{FFT}, ε, and N_{az}. Figures 1-3 are taken from the "base case" having N=7680 macroparticles, $N_{FFT} \times N_{FFT} = 32 \times 32$ FFT grid cells, ε =4.42mm (> cell size at all azimuths), and N_{az}=488 steps/turn . Convergence studies included the following ranges of parameters:

- N =7680, 30720, 122880, 245760
- $N_{FFT} \times N_{FFT} = 32 \times 32, 64 \times 64, 128 \times 128$
- ε=6.25, 4.42, 3.125mm
- N_{az} = 488, 880

In the macroparticle variation, the main effects of increasing the number of macroparticles are a delay in the onset of the instability and a faster rise of the instability following onset. The initial and final configurations are basically unchanged as are the main features of the evolution. The same effect is observed when the number of FFT grid points is increased. In both of these cases, the passage to higher resolution decreases the numerical viscosity, thus sharpening the observed evolution.

Choice of the smoothing parameter is perhaps one of the more subjective aspects of PIC calculations by our chosen method. Too small a value obscures the collective dynamics in noise due to binary interactions of macroparticles with nearby FFT nodes. Too large a value smooths away the dynamics. As a guiding constraint, we maintained the values of the smoothing parameter to be larger than the FFT cell size in all cases. As the value of the smoothing parameter was varied, it was observed that increasing the smoothing parameter results in a decreased saturation level of the instability, both in terms of rms emittances and fraction of beam particles in the halo.

Finally, increasing the number of azimuthal integration points resulted in no basic changes in the results.

In order to illustrate the effects of the numerical parameter variations, we now compare the beam evolution for the "base case" and a "big case" having the following parameter values: N = 245760 macroparticles, $N_{FFT} \times N_{FFT} = 128 \times 128$ FFT grid cells, ε = 4.42mm, and N_{az} = 880 steps/turn. In both cases the main features of the beam evolution are the same. In the "big case" the onset of instabiltiy is delayed, the growth of the instability is faster, and the beam halo at saturation contains a slightly higher fraction of the beam. Figure 4 shows the beam averages of $<(\Delta x)^2>$ and $<(\Delta y)^2>$ for the two cases plotted versus turn number. The most noticeable difference is in the decrease of the vertical fluctuations driving the instability. In the "big case" this decrease is both delayed and sharper relative to the "base case". Figure 5 plots the evolution of the rms y emittances for the two cases, and it is again seen that the rise in the emittance for the "big case" is delayed but sharper in comparison with the "base case". The difference in saturation value of the two emittances is very small, with that of the "big case" being slightly larger.

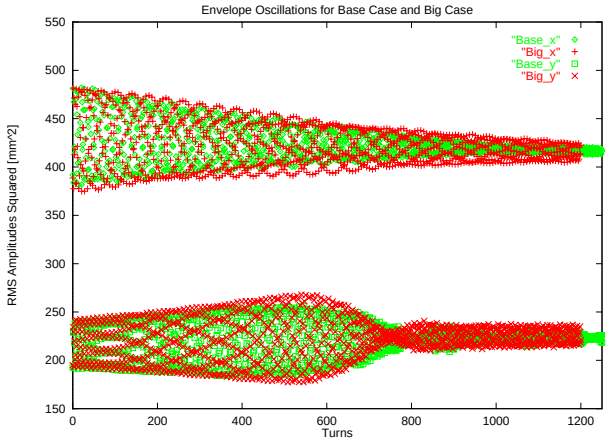

Figure 4. Average values of $<(\Delta x)^2>$ and $<(\Delta y)^2>$ plotted once each turn and showing envelope oscillations. Plots are for the "base case" and the "big case".

4 DISCUSSION AND CONCLUSIONS

Convergence studies have been carried out for the calculation of halo generation via the parametric resonance driven by rms mismatch. In these studies the number of macroparticles per FFT grid cell varied from a minimum of 7.5 to a maximum of 30, although the effective number in the occupied cells is at least four

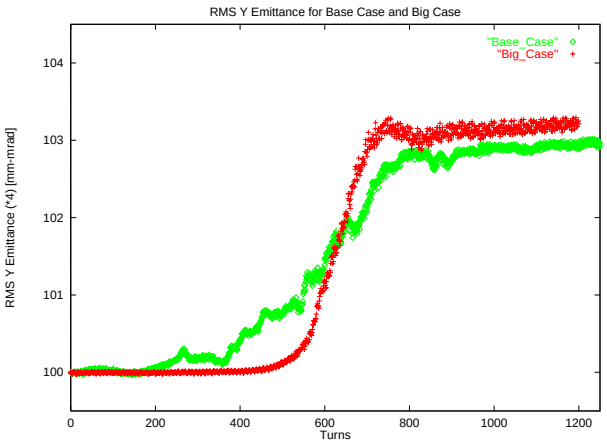

Figure 5. Transverse rms emittances ε_y versus turn number for the "base case" and the "big case".

times higher since the FFT grid is twice the extent of the beam in both directions. The number of integration points per quadrupole pair is 20 in the case of 488 integration steps and 37 for 880 steps. It was found that the "base case" of 7680 macroparticles resulted in a reasonable description of the overall dynamics of the beam. Increased resolution revealed a delay in the onset of the instability together with a faster rise time. However, in the case studied here more than 1% of the beam macroparticles migrated to the halo and the vertical rms emittance growth was more than 3%. In high intensity rings, such as SNS, the limit on uncontrolled losses is 10^{-4}, or two orders of magnitude below the observed losses here. To accurately calculate the dynamics of cases with such small losses, high resolution will be a requirement.

In order to perform high resolution calculations in a routine fashion, we will require greater computing resources than have been used here. The present calculations were performed on a variety of IBM RS-6000 and DEC Alpha workstations. The fastest of these machines was a 400MHz Alpha, and the timings on this machine were: approximately 2 turns/minute, or 10 hours for 1250 turns, for the "base case"; and about 3 turns/hour, or 400 hours for 1250 turns, for the "big case". In order to perform high resolution calculations routinely, we have taken two steps: we have obtained accounts at NERSC, and we have assembled our own parallel computer, the SNS Wonderland Cluster. This cluster consists of five 533 MHz DEC Alpha computers (one gateway node and four compute nodes), each with 4MB of 9ns SRAM Cache, 256MB memory, 4.5GB SCSI Hard Drive, and 10/100 Ethernet. The gateway node contains an additional 18GB storage, and the cluster is connected by a 10/100 Ethernet switch. The cluster is running the RedHat Linux operating system and supports PVM and MPI message passing interfaces. Because particle tracking calculations are CPU and cache bound, the 533MHz processor speed and 4MB cache are well chosen.

Also, the cluster is easily upgradeable, so that more compute power can be added when desired.

5 ACKNOWLEDGEMENT

* Research on the Spallation Neutron Source is sponsored by the Division of Materials Science, U.S. Department of Energy, under contract number DE-AC05-96OR22464 with Lockheed Martin Energy Research Corporation for Oak Ridge National Laboratory.

REFERENCES

[1] National Spallation Neutron Source Conceptual Design Report, Volumes 1 and 2, NSNS/CDR-2/V1,2, (May, 1997); On the World Wide Web at http://www.ornl.gov/~nsns/CDRDocuments/CDR.html

[2] R. W. Hockney and J. W. Eastwood, *Computer Simulation Using Particles*, Adam Hilger, IOP Publishing Ltd. (New York: 1988); C. K. Birdsall and A. B. Langdon, *Plasma Physics via Computer Simulation*, McGraw-Hill Book Company (New York: 1985).

[3] Jones, F., *Users' Guide to ACCSIM*, TRIUMF Design Note TRI-DN-90-17, (1990).

[4] J. S. O'Connell, T. P. Wangler, R. S. Mills, and K. R. Crandall, Proc. 1993 Part. Accel. Conf., Washington, DC (1993) 3657; J. M. Lagniel, Nucl. Inst. Meth. A345 (1994) 46; J. M. Lagniel, Nucl. Inst. Meth. A345 (1994) 405; R. L. Gluckstern, Phys. Rev. Lett. 73 (1994) 1247.